

Carbonate chemistry in the microenvironment within cyanobacterial aggregates under present-day and future $p\text{CO}_2$ levels

Meri Eichner ^{1,2*} Dieter Wolf-Gladrow ³ Helle Ploug ²

¹Centre Algatech, Institute of Microbiology of the Czech Academy of Sciences, Třeboň, Czech Republic

²Department of Marine Sciences, University of Gothenburg, Gothenburg, Sweden

³Alfred Wegener Institute Helmholtz Centre for Polar and Marine Research, Bremerhaven, Germany

Abstract

Photosynthesis and respiration cause distinct chemical microenvironments within cyanobacterial aggregates. Here, we used microsensors and a diffusion–reaction model to characterize gradients in carbonate chemistry and investigate how these are affected by ocean acidification in Baltic vs. Pacific aggregates (*Nodularia* and *Dolichospermum* vs. *Trichodesmium*). Microsensor measurements of O_2 and pH were performed under in situ and expected future $p\text{CO}_2$ levels on *Nodularia* and *Dolichospermum* aggregates collected in the Baltic Sea. Under in situ conditions, O_2 and pH levels within the aggregates covered ranges of 80–175% air saturation and 7.7–9.4 in dark and light, respectively. Carbon uptake in the light was predicted to reduce HCO_3^- by 100–150 $\mu\text{mol L}^{-1}$ and CO_2 by 3–6 $\mu\text{mol L}^{-1}$ in the aggregate center compared to outside, inducing strong CO_2 depletion (down to 0.5 $\mu\text{mol L}^{-1}$ CO_2 remaining in the center) even when assuming that HCO_3^- covered 80–90% of carbon uptake. Under ocean acidification conditions, enhanced CO_2 availability allowed for significantly lower activity of carbon concentrating mechanisms, including a reduction of the contribution of HCO_3^- to carbon uptake by up to a factor of 10. The magnification of proton gradients under elevated $p\text{CO}_2$ that was predicted based on a lower buffer capacity was observed in measurements despite a concurrent decrease in photosynthetic activity. In summary, we provide a quantitative image of the inorganic carbon environment in cyanobacterial aggregates under present-day and expected future conditions, considering both the individual and combined effects of the chemical and biological processes that shape these environments.

As the oceans are absorbing a significant part of anthropogenic CO_2 emissions, seawater pH levels are continuously decreasing, a phenomenon referred to as ocean acidification (Doney et al. 2009). The change in pH for a given amount of CO_2 uptake differs depending on the chemical properties of the seawater, including the initial carbon content (Eggleston et al. 2010) and alkalinity (defined as the excess of proton acceptors over proton donors; Dickson et al. 2007).

The Baltic Sea is a semi-enclosed brackish water system characterized by strong regional and seasonal variability in seawater chemistry. The strong salinity gradient from its inlet to the northern tip (35 to 3; Müller et al. 2016) is associated with large gradients in dissolved inorganic carbon (DIC; > 2000–600 $\mu\text{mol kg}^{-1}$; Schneider et al. 2015) and total alkalinity (> 2500–600 $\mu\text{mol kg}^{-1}$; Müller et al. 2016). The low total alkalinity as compared to open ocean water means a lower capacity to take up CO_2 , but also a lower capacity to buffer changes in pH due to CO_2 uptake (Zeebe and Wolf-Gladrow 2001). Every summer, dense cyanobacterial blooms dominated by the filamentous, aggregate-forming, N_2 -fixing cyanobacteria *Nodularia spumigena* (hereafter *Nodularia*), *Dolichospermum* sp. (previously classified as *Anabaena* sp.), and *Aphanizomenon* sp. appear in the Baltic Sea. Photosynthetic CO_2 uptake by these blooms induces strong variation in $p\text{CO}_2$ and pH levels over the yearly cycle, with a pH range from 7.9 in winter to 8.5 in summer (Wesslander et al. 2010), and a $p\text{CO}_2$ range from ca. 100 μatm in winter to ca. 500 μatm in summer (Omstedt et al. 2014).

Aside from this regional and seasonal variability, considerable variability on the microscale is caused by the formation of

*Correspondence: eichner@alga.cz

This is an open access article under the terms of the Creative Commons Attribution-NonCommercial License, which permits use, distribution and reproduction in any medium, provided the original work is properly cited and is not used for commercial purposes.

Additional Supporting Information may be found in the online version of this article.

Author Contribution Statement: All authors contributed substantially to the study's conception. ME performed experiments and data analysis and applied the model. DWG developed the model. ME drafted the initial version of the manuscript, all authors contributed to manuscript writing and approved the final submitted manuscript.

cyanobacterial aggregates. Microsensor studies have revealed distinct microenvironments within aggregates with regard to nutrients, O₂ concentrations, and pH levels (Ploug 2008; Ploug et al. 2011; Klawonn et al. 2015). Variations in pH, in turn, can have multiple feedbacks on physiology as they affect the requirements for regulatory mechanisms to maintain pH homeostasis and are associated with changes in nutrient availability, including shifts in iron speciation and dissolution (Morel and Hering 1993; Millero et al. 2009) as well as carbonate chemistry (Zeebe and Wolf-Gladrow 2001). Specifically, the increase in pH levels observed in the light suggests that CO₂ may become depleted within aggregates. While most cyanobacteria (including *Trichodesmium* and *Anabaena*; Badger et al. 2006) can take up HCO₃⁻ in addition to CO₂, HCO₃⁻ uptake is energetically more costly, hence a drawdown of CO₂ within the aggregate microenvironment can be expected to feed back on cellular energy budgets (Eichner et al. 2015).

The concentrations of CO₂ and HCO₃⁻ in the vicinity of the cell depend on the interplay between carbon fluxes in and out of the cell (i.e., photosynthesis and respiration), the chemical equilibrium reactions, which may be enzymatically accelerated by extracellular carbonic anhydrase (eCA), and the diffusion of these molecules within the aggregate microenvironment. The concentration gradients of individual carbon species around plankton cells have been modeled as a function of bulk seawater carbonate chemistry, biological carbon fluxes, the equilibrium reactions and the diffusion rates (Wolf-Gladrow and Riebesell 1997). Application of such calculations has advanced our understanding of cellular carbon acquisition mechanisms in diatoms (Chrachri et al. 2018) and showed that with increasing ocean acidification, as the buffer capacity of seawater decreases, the variations in microenvironment pH around phytoplankton cells will increase in magnitude (Flynn et al. 2012). For the diffusive boundary layer around aggregates of the N₂ fixer *Trichodesmium*, strong deviations in pH, aragonite saturation state, as well as DIC levels compared to the surrounding seawater have been predicted (Kranz et al. 2010). Even stronger variations in microenvironment carbonate chemistry may be expected for cyanobacterial aggregates in the Baltic Sea, due to their larger size and accordingly thicker diffusive boundary layers and the low alkalinity of Baltic seawater compared to open ocean systems.

Previous ocean acidification studies have shown that different species of N₂ fixers diverge strongly in their responses to elevated pCO₂ (Eichner et al. 2014b). Accounting for this diversity in ocean acidification responses is a key requirement for improving model predictions of global change effects on primary productivity, yet, we are only starting to appreciate and understand this diversity. One potential explanation for the different responses of Baltic vs. open ocean diazotroph species is that Baltic cyanobacteria are adapted to highly variable microenvironments in terms of carbonate chemistry and thus less susceptible to the changes related to ocean acidification.

Here, we systematically analyzed carbonate chemistry in the microenvironment of cyanobacterial aggregates under present-day and future pCO₂ levels. Using microsensors, we measured O₂ and pH gradients in and around cyanobacterial aggregates collected in the Baltic Sea, firstly under in situ conditions and then investigating instantaneous as well as acclimation responses to elevated bulk pCO₂ levels. In a next step, we applied a diffusion–reaction model (Wolf-Gladrow and Riebesell 1997; Wolf-Gladrow et al. 1999) to these data for describing full carbonate chemistry gradients within the aggregate microenvironments. In these model calculations, we compared the effects of elevated pCO₂ levels in different seawater chemistry scenarios representing Baltic Sea and Pacific conditions. Application of the model to previously published microsensor data on the tropical aggregate-forming cyanobacterium *Trichodesmium* then allowed us to extend our predictions of microenvironment carbonate chemistry to a wider range of aggregate-forming cyanobacteria under various seawater conditions.

Material and methods

Sampling

Experiments were performed between 31 July and 22 August 2015 at Askö Laboratory in the Stockholm Archipelago. Aggregates and seawater were sampled at station B1 (58°48'118"N, 17°37'507"E) during the onset of a *Nodularia* bloom. Salinity at the study site was ~6 (practical salinity units [psu]). Aggregates of *Nodularia* and *Dolichospermum* were sampled by net-tows (41 μm mesh size) in the upper 3 m, or with a bucket from the surface, depending on aggregate density. On one occasion (05 August), sampling took place further out into the open Baltic (58°43'38"N, 17°45'41.3"E, Landsort deep) with a 90 μm net from the upper 5 m. Samples were taken to the laboratory immediately after sampling and single aggregates were picked with a Pasteur pipette under a stereomicroscope at 2X magnification (Olympus SZ61, LRI Instrument AB). Aggregates were then kept at 15°C and 250 μmol photons m⁻² s⁻¹ (4000 K) at pH 8.2 until the start of measurements within a few hours.

While in situ temperatures rose from ~15°C to ~18°C over the course of the study, all incubations and measurements were conducted at 15°C for better comparability between treatments and replicates performed over time. In parallel with aggregate sampling, samples for in situ pH, DIC and total alkalinity in surface water were taken in a 1-liter flask filled without headspace, reducing air contact and agitation during sampling. Carbonate chemistry samples were processed directly upon reaching the laboratory.

Carbonate chemistry measurements

pH was measured at 15°C with pH microelectrodes calibrated with NBS buffers (Sigma Aldrich). Samples for DIC and total alkalinity were filtered through 0.2 μm syringe filters (Filtropur S, Sarstedt) and stored at 4°C until measurements.

DIC was measured colorimetrically (QuAatro autoanalyzer, Seal) and total alkalinity was determined by potentiometric titration (TitroLine alpha plus, Schott Instruments) at Alfred Wegener Institute, Bremerhaven, Germany. $p\text{CO}_2$ in the manipulated seawater was calculated from pH and DIC using the CO2sys template (Pierrot et al. 2006).

Incubations and carbonate chemistry manipulation

Aggregates were incubated at two different $p\text{CO}_2$ levels for 3–4 d at 15°C and 250 $\mu\text{mol photons m}^{-2} \text{s}^{-1}$ (light source VWR Sverige AB; light sensor QSL 2101, Biospherical Instruments). In order to avoid diffusion limitation and maintain aggregates intact for the duration of the incubations, incubation vials (glass serum bottles of 165 mL filled without headspace) were mounted in a roller tank (ca. 20 cm diameter) rotating on a custom-made roller table (ca. 2 rpm). Seawater for incubations was sampled from station B1 not more than 3 d before the start of incubations and prebubbled with air of the respective $p\text{CO}_2$ overnight or until the pH had reached a stable value. CO_2 gas mixtures were prepared with gas mixing pumps (H. Wösthoff GmbH) from pure CO_2 (Strandmöllen AB) and CO_2 -depleted air, which was generated by passing compressed air consecutively through air tight flasks containing NaOH (1 M) and soda lime with a pH indicator dye (Sigma-Aldrich). Equilibrated seawater was carefully filled into serum bottles with a syringe fitted with a tube reaching to the bottom of the flask. Between 6 and 14 aggregates were added depending on their size, aiming to achieve similar biomass in all incubation vials.

Subsamples for pH, DIC, and total alkalinity were taken from the seawater in incubation vials at the beginning and the end of all incubations. Carbonate chemistry during the incubations as determined from these samples is shown in Table S1. Total alkalinity was not significantly different between the beginning and the end of incubations (t -test, $p > 0.05$, $n = 3$ –4), whereas DIC consumption over the incubation time was $91 \pm 35 \mu\text{mol kg}^{-1}$, inducing a pH increase by 0.28 ± 0.14 . In controls with unfiltered seawater without aggregates that were incubated in parallel, DIC decreased by $37 \pm 35 \mu\text{mol kg}^{-1}$ and pH increased by 0.09 ± 0.14 . Tests with filtered seawater showed no appreciable change in pH during handling and over the incubation period (data not shown). At the end of incubations, individual aggregates relatively similar in size were picked for microsensor measurements.

Microsensor measurements

For microsensor measurements, single aggregates were placed in a custom-made flow system (Ploug and Jørgensen 1999) under a flow of roughly 0.1 mm s^{-1} and fixed with a thin glass needle to keep them in position. The flow system was placed in an aquarium filled with filtered ($0.2 \mu\text{m}$) seawater maintained at 15°C using a thermostated water bath. Light intensity was adjusted to 150–250 $\mu\text{mol photons m}^{-2} \text{s}^{-1}$. Test measurements showed that this range of light intensities caused variations at the aggregate surface by not

more than 15 $\mu\text{mol L}^{-1} \text{O}_2$ and 0.1 pH units, respectively. Prior to measurements, carbonate chemistry of the seawater in the system was adjusted by bubbling with air of the respective $p\text{CO}_2$ until the desired pH value was reached. For testing short-term effects of altered carbonate chemistry, conditions were gradually changed by bubbling over a period of 1–2 h while the cyanobacterial aggregate was in the system. Measurements were started once the pH level was stable at the desired level for ~ 30 min.

To test for potential adverse effects of incubating the aggregates in the flow system during microsensor measurements and/or effects of the intrinsic diel cycle on the photosynthetic activity, O_2 concentrations and pH levels at the surface of an aggregate were monitored in a long-term measurement over 10 h. Over this time period, O_2 concentrations at the aggregate surface decreased by 50 $\mu\text{mol L}^{-1}$ (at an average concentration in the light of $\sim 150 \mu\text{mol L}^{-1}$ above bulk conditions) presumably due to a decrease in photosynthetic activity, while pH ranged between 8.35 and 8.45 (at an average value in the light of ~ 0.5 pH units above bulk). The maximum changes over the duration of one set of measurements (max. 2 h) were 10 $\mu\text{mol L}^{-1} \text{O}_2$ and 0.1 pH units. Thus, the drift in O_2 and pH as well as the effects of the diel cycle on replicates analyzed at different times of the day were considered negligible.

Consecutive measurements of pH and O_2 were performed on 21 aggregates in total. pH was measured with a pH microelectrode (Unisense, tip size 100 μm , response time < 10 s). O_2 profiles were measured with O_2 electrodes (Unisense, tip size 10 μm , response time 1–3 s) that were calibrated with seawater saturated with air and N_2 (AGA). Upon switching between light and dark profiles, cells were allowed to acclimate for 10 min or until pH or O_2 at the surface of the aggregate had stabilized. O_2 and pH were measured in 100 μm steps from about 1 mm above the aggregate to the center (until the maximum/minimum was passed). The analytic solutions to the reaction–diffusion equation inside the aggregate and the diffusion equation within the diffusive boundary layer were fitted to these depth profiles in order to calculate net O_2 fluxes (J) from steady state O_2 gradients at the aggregate surface (dC/dr) as described previously (Ploug et al. 1997), assuming spherical geometry. The calculation was based on Fick's 1st law of diffusion, applying a diffusion coefficient (D) of $1.81 \times 10^{-5} \text{ cm}^2 \text{ s}^{-1}$ (15°C, salinity 6; Broecker and Peng 1974):

$$J = -D \times dC/dr$$

Diffusion–reaction model

Gradients of CO_2 , HCO_3^- , H^+ , and O_2 within the aggregate microenvironment were modeled using the model described by Wolf-Gladrow and Riebesell (1997; here extended by inclusion of O_2), which accounts for the diffusion of each of these compounds in the aggregate microenvironment as well as the reactions in the carbonate system (Fig. 1). Reaction

coefficients were taken from Zeebe and Wolf-Gladrow (2001). As input parameters, pH and O_2 concentrations measured with microsensors in the surrounding seawater for each individual aggregate, as well as average values of total alkalinity and DIC measured in bulk seawater during the study period were used (Table S2). Total carbon uptake by the aggregates was based on O_2 evolution rates calculated from measured O_2 gradients as described above (Microsensor measurements), using the photosynthetic quotients (PQ) specified for each aggregate in the text and figure legends.

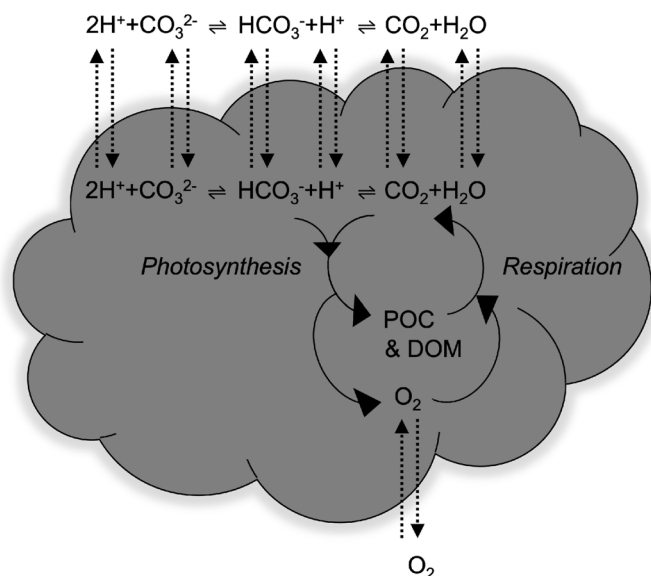


Fig 1. Conceptual overview of the major biological, physical, and chemical processes shaping gradients of O_2 , pH, and inorganic carbon in the microenvironment of cyanobacterial aggregates. POC, particulate organic carbon; DOM, dissolved organic matter. Solid arrows indicate chemical transformations; dotted arrows indicate diffusion.

Following the more conservative estimates of HCO_3^- contribution to total carbon uptake based on membrane inlet mass spectrometry measurements on *Trichodesmium* in previous studies (Rost et al. 2007; Kranz et al. 2009; Eichner et al. 2015), we assumed a contribution of 80% HCO_3^- to total carbon uptake unless specified otherwise.

Note that in standard runs of the model we assumed no eCA activity, in line with published conceptual models of the cyanobacterial carbon concentrating mechanism (CCM; Badger and Price 2003; Price et al. 2008; Burnap et al. 2015; Long et al. 2016; Kaplan 2017) and measurements of very low activity of eCA in *Trichodesmium* (Kranz et al. 2009). Hence, in these model runs, chemical equilibration within the diffusive boundary layer is slower than diffusion, in contrast to previous model calculations (Flynn et al. 2012). Additionally, a sensitivity analysis testing different levels of eCA activity was performed (see Supplementary Material).

Results

Cyanobacterial abundance and in situ carbonate chemistry

Over the course of the study (19 d), density and species composition of the large filamentous cyanobacteria changed considerably (Table 1). During the first part of the study, *Nodularia* was absent and *Dolichospermum* was present only at relatively low density. In the middle of the study period, *Dolichospermum* gradually increased in density, while a surface bloom of *Nodularia* developed rapidly, with dense surface aggregations appearing (Fig. 2a), followed by a phase of high density in *Dolichospermum*, and a second peak in *Nodularia* occurrence. Concurrently, in situ pH levels increased from 8.2 to a maximum of 8.6, while DIC concentrations decreased from ca. $1420 \mu\text{mol kg}^{-1}$ to ca. $1290 \mu\text{mol kg}^{-1}$, equivalent to a $p\text{CO}_2$ decline from ca. 350 to $130 \mu\text{atm}$ (Table 1).

Table 1. In situ carbonate chemistry and estimated cyanobacterial abundance over the course of the study. $p\text{CO}_{2_calc}$ was calculated from dissolved inorganic carbon (DIC) and pH. For total alkalinity (TA) and DIC, average \pm SD of duplicate measurements are shown. “Surface bloom” denotes accumulation of *Nodularia* at the surface. “Landsort deep” denotes different sampling location (see the Methods section). Aggregate density is based on visual estimation from net samples. n.a., not available.

Date	pH _{NBS}	TA	DIC	$p\text{CO}_{2_calc}$	Aggregate abundance		Comment
		$\mu\text{mol kg}^{-1}$	$\mu\text{mol kg}^{-1}$		<i>Dolichosp.</i>	<i>Nodularia</i>	
03 Aug	8.24	1543 \pm 15	1415 \pm 1	340	+		
04 Aug	8.23	1553 \pm 12	1419 \pm 1	349	+		
05 Aug	8.18	n.a.	1390 \pm 1	384	+		Landsort deep
07 Aug	8.36	1529 \pm 2	1382 \pm 0	250			
09 Aug	8.37	1553 \pm 5	1393 \pm 0	246	++	++++	Surface bloom
10 Aug	8.43	1536 \pm 4	1361 \pm 0	208	+++		
11 Aug	8.56	1568 \pm 39	1367 \pm 1	152	++++	++	
19 Aug	8.59	1479 \pm 1	1294 \pm 3	134			
21 Aug	8.41	1528 \pm 27	1288 \pm 1	206		++++	Surface bloom
22 Aug	8.59	1478 \pm 2	1293 \pm 1	133	++	+++	

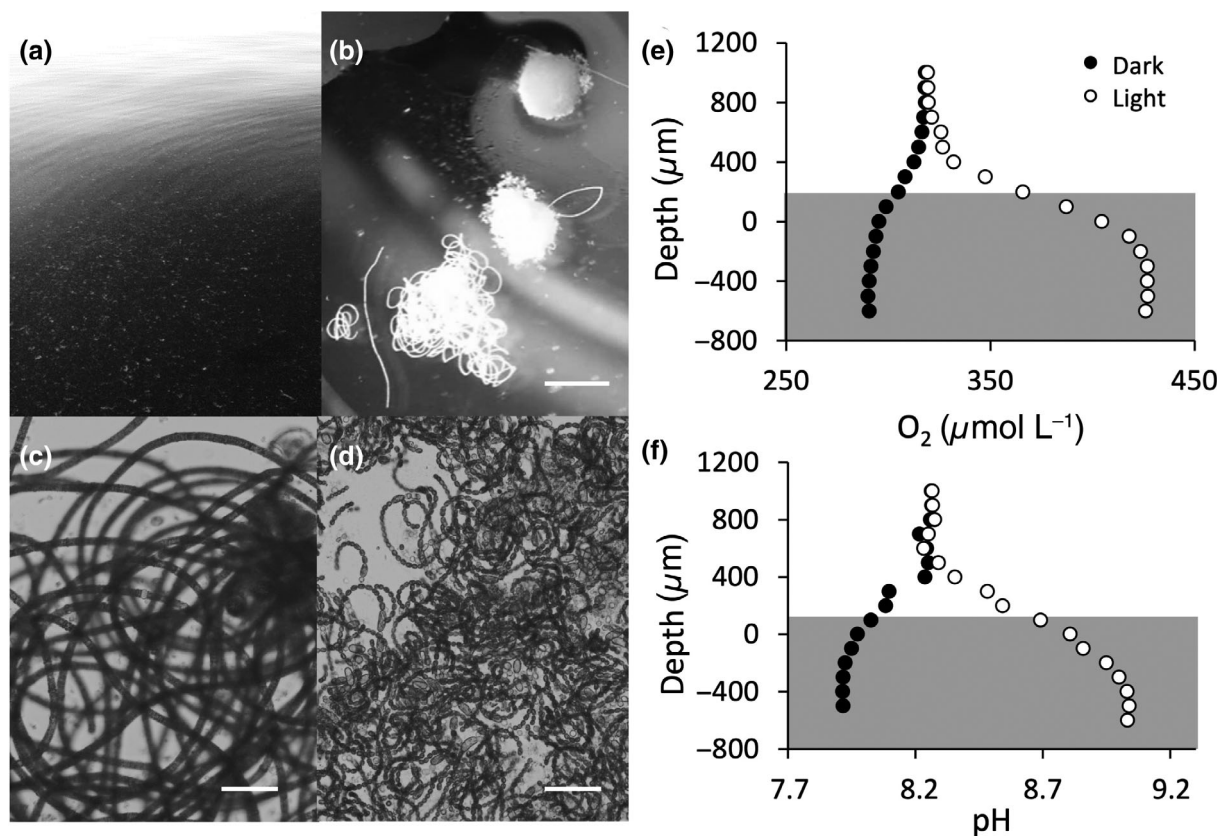


Fig 2. Typical appearance and depth profiles of O₂ and pH of cyanobacterial aggregates analyzed in this study. (a) Surface accumulation of *Nodularia* aggregates. (b) Two aggregates of *Dolichospermum* (middle and top) and an aggregate of *Nodularia* (bottom). Scale bar: 2 mm. (c, d) Close-ups of *Nodularia* (c) and *Dolichospermum* (d) aggregates. Scale bars: 50 μm. (e, f) Typical depth profiles of O₂ (e) and pH (f) measured in light and dark under in situ pCO₂ on a freshly collected aggregate of *Nodularia*. Approximate area taken by the aggregate is indicated by gray shading.

O₂ and pH microenvironments under present-day conditions

In the first set of measurements, pH and O₂ gradients were characterized on freshly collected aggregates of *Nodularia* and *Dolichospermum* under bulk pCO₂ and pH levels representative of the conditions at the time of sampling. Following the development of species composition and in situ carbonate chemistry over the study period (Table 1), measurements on *Dolichospermum* were thus conducted at a pH of 8.2–8.3, while measurements on *Nodularia* were mostly conducted at a higher pH of 8.5–8.6 (Table 2).

O₂ concentrations and pH levels showed strong light-dependent gradients in and around aggregates of both *Nodularia* and *Dolichospermum* as a result of photosynthesis and respiration (Fig. 2e,f). The total range of O₂ concentrations observed in these aggregates under present-day in situ pCO₂ was 239 μmol L⁻¹ (measured in the dark) to 532 μmol L⁻¹ (measured in the light), equivalent to a range from 80% to 175% air saturation, with average levels of 90% air saturation in the dark and 140% air saturation in the light (Table 2). pH values within aggregates ranged between 7.7 (measured in the dark) and 9.4 (measured in the light) among all aggregates, and was

equivalent to an average difference in proton concentration between light and dark of 11 ± 5 nmol L⁻¹. Except for pH in the light, which was higher in *Nodularia* (*t*-test, $p < 0.05$, $n = 3-4$), and O₂ concentration in the dark, which was lower in *Nodularia* (*t*-test, $p < 0.05$, $n = 3-4$), conditions in the aggregate center were not significantly different between *Dolichospermum* and *Nodularia* (*t*-test, $p > 0.05$, $n = 3-4$).

O₂ uptake and production by the aggregates, as calculated from steady state O₂ gradients at the aggregate surface in dark and light, were on average 1.8 ± 1.5 and 4.8 ± 4.5 nmol h⁻¹ aggregate⁻¹, respectively, and were not significantly different between species (*t*-test, $p > 0.05$, $n = 3-4$; Table 2). Similarly, volume-specific rates of O₂ uptake and production were not significantly different between species (*t*-test, $p > 0.05$, $n = 3-4$; Table 2). Respiration and photosynthesis were highly correlated for individual aggregates of both species, with respiration accounting to approximately a third of gross photosynthesis (estimated as the sum of net O₂ fluxes in light and dark; Fig. S1, also cf. data in Table 2). The average volume of *Dolichospermum* and *Nodularia* aggregates was not significantly different (*t*-test, $p > 0.05$, $n = 3-14$; Table S3). However, the average chlorophyll (Chl) *a* content per aggregate was about

Table 2. Conditions in the center of freshly collected aggregates of *Dolichospermum* and *Nodularia* as well as O₂ evolution (light) or uptake (dark) rates measured under present-day in situ conditions. d[H⁺] indicates the difference in H⁺ concentration in light vs. dark; n.a., not available.

Species	ID	Bulk pH	Light cond.	pH in center	d[H ⁺] in center	[O ₂] in center	O ₂ evolution or uptake rate		
							nmol h ⁻¹ aggr. ⁻¹	nmol h ⁻¹ mm ⁻³	
					nmol L ⁻¹	μmol L ⁻¹			
<i>Dolichospermum</i>	D1	8.2	Light	8.8	12	402	1.7	4.6	
			Dark	7.9		322	0.6	3.5	
	D2	8.3	Light	8.7	6	347	1.0	2.6	
			Dark	8.1		289	0.6	2.3	
	D3	8.3	Light	9.0	11	427	4.5	7.1	
			Dark	7.9		290	1.3	1.5	
	Avg ± SD			Light	8.9±0.2	10±3	392±41	2.4±1.9	4.7±2.3
				Dark	8.0±0.1		300±19	0.8±0.4	2.4±1.0
<i>Nodularia</i>	N1	8.2	Light	9.0	18	375	0.7	21.0	
			Dark	7.7		264	1.3	6.3	
	N2	8.6	Light	9.3	3	455	4.0	10.5	
			Dark	8.4		242	2.3	2.7	
	N3	8.5	Light	9.4	15	489	10.1	7.7	
			Dark	7.8		239	4.6	1.3	
	N4	8.6	Light	9.4	n.a.	532	11.9	9.2	
			Dark	n.a.		n.a.	n.a.	n.a.	
	Avg ± SD			Light	9.2±0.2	12±8	463±66	6.7±5.2	12.1±6.1
				Dark	8.0±0.4		249±14	2.7±1.7	3.4±2.5
Total	Avg ± SD		Light	9.1±0.3	11±5	432±65	4.8±4.5	8.9±6.0	
			Dark	8.0±0.2		274±32	1.8±1.5	2.9±1.8	

twice as high in *Nodularia* as in *Dolichospermum* (Table S3), implying a higher photosynthetic activity per unit of Chl *a* in *Dolichospermum*.

O₂ and pH levels were also compared to previous results on *Trichodesmium*, which has a notably smaller average volume than the Baltic aggregates (by about a factor of 5; Table S3), implying a smaller biologically active volume and shorter diffusion distance to the center of the aggregate. While absolute O₂ concentrations differed according to the different O₂ solubility in Baltic Sea vs. Pacific seawater, O₂ levels relative to air saturation in the center of aggregates were very similar between *Trichodesmium* and Baltic aggregates despite the size difference (Tables S3, S4; *t*-test, *p* > 0.05, *n* = 3–10). pH values in the center of aggregates were somewhat higher in the Baltic aggregates than in *Trichodesmium* (significant difference only in light, Table S4; *t*-test, *p* < 0.05, *n* = 5–10), while the range in proton concentrations in light vs. dark was similar among them (Table S4; *t*-test, *p* > 0.05, *n* = 5–8). Average O₂ production and uptake rates per aggregate were variable and not significantly different between Baltic and *Trichodesmium* aggregates (Table S4; *t*-test, *p* > 0.05, *n* = 3–10). Given the size difference between the aggregate types, the similar rates per aggregate reflect lower volume-specific rates of photosynthesis

and respiration in the Baltic aggregates, which was statistically significant for ambient *p*CO₂ levels (Table S4; *t*-test, *p* < 0.05, *n* = 6–10) but not for future *p*CO₂ levels (Table S4; *t*-test, *p* > 0.05, *n* = 3–7). This difference in volume-specific rates might be due to deviations in biomass per volume, physiological state, or diffusion limitation of respiration and/or photosynthesis in the larger aggregates of *Nodularia* and *Dolichospermum* (Ploug et al. 2011).

Microenvironment carbonate chemistry under present-day conditions

In a next step, concentration gradients of the individual carbon species within the aggregate microenvironment were modeled based on size and O₂ evolution rates of individual aggregates (Table 2; Eichner et al. 2017) as well as chemical and physical conditions in the bulk seawater (DIC, pH, total alkalinity, O₂, salinity, temperature; Table S2). Measured and modeled O₂ and pH levels for *Dolichospermum* and *Nodularia* aggregates under Baltic seawater conditions as well as for *Trichodesmium* under Pacific conditions are shown in Fig. 3.

For a relatively small and low activity *Dolichospermum* aggregate (ID D2) sampled under prebloom conditions (bulk pH 8.2), these calculations predict reduced HCO₃⁻ and CO₂

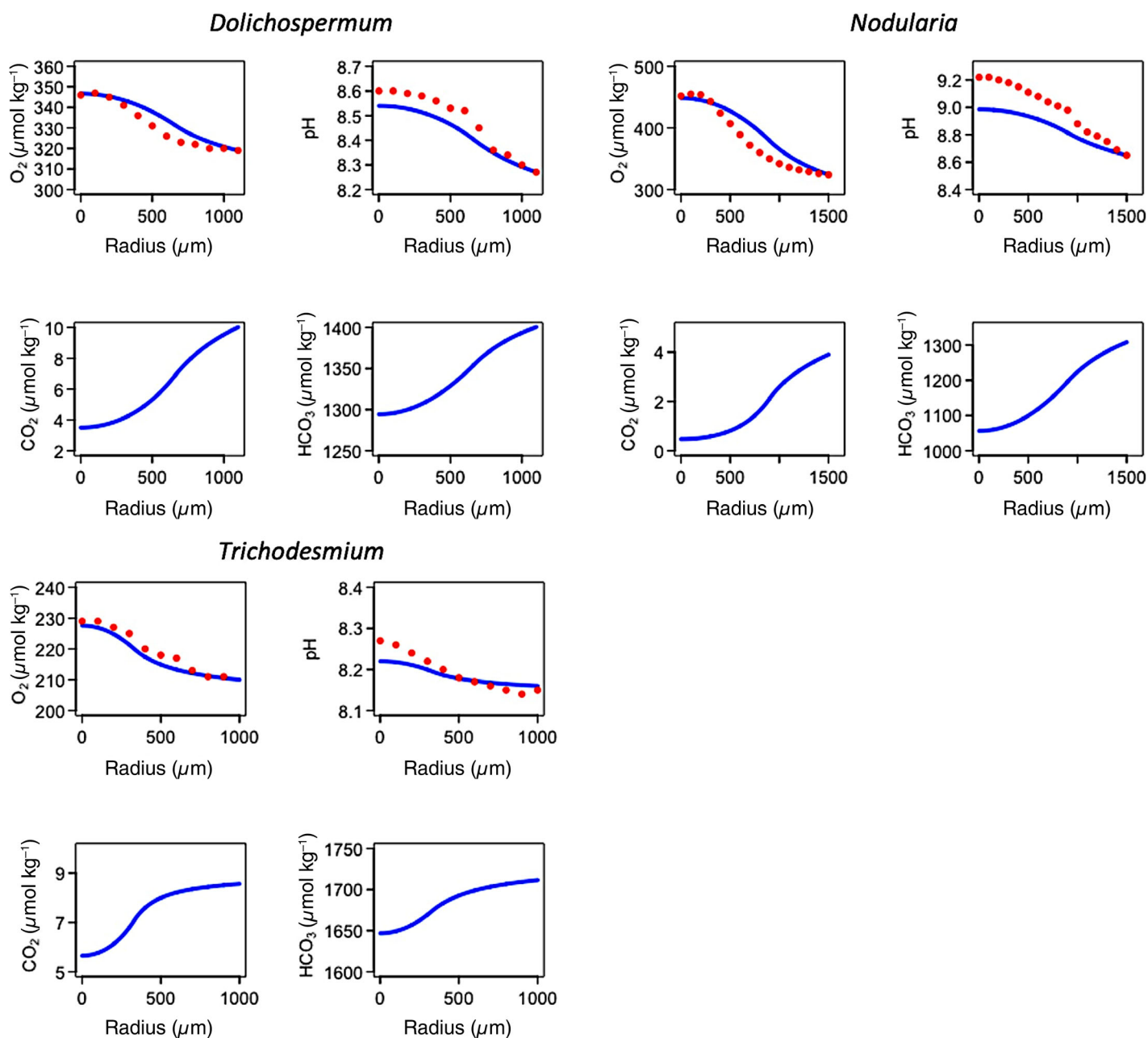


Fig 3. Modeled gradients of O_2 , pH, CO_2 , and HCO_3^- concentrations (blue lines) and measured O_2 and pH values (red circles) in the microenvironments of three representative cyanobacterial aggregates. *Dolichospermum* ID D2, PQ 0.8, 20% CO_2 uptake, total C uptake 4.51×10^{-13} mol C aggregate $^{-1}$ s $^{-1}$; *Nodularia* ID N2, PQ 1.7, 10% CO_2 uptake, total C uptake 7×10^{-13} mol C aggregate $^{-1}$ s $^{-1}$; *Trichodesmium* ID T1, PQ 0.8, 20% CO_2 uptake, 1.8×10^{-13} mol C aggregate $^{-1}$ s $^{-1}$. Other input parameter values as specified in Table S2. Note different scales of y-axes.

concentrations in the aggregate center due to cellular carbon uptake by ca. $100 \mu\text{mol L}^{-1}$ HCO_3^- and $6 \mu\text{mol L}^{-1}$ CO_2 , reaching a CO_2 concentration of $3.5 \mu\text{mol L}^{-1}$ in the center when assuming a $CO_2 : HCO_3^-$ uptake ratio of 20% : 80%. For a more productive *Nodularia* aggregate (ID N2) sampled under bloom-conditions (bulk pH 8.6), the model predicts a decrease in HCO_3^- of ca. $150 \mu\text{mol L}^{-1}$ and $3.5 \mu\text{mol L}^{-1}$ CO_2 in the aggregate center, reaching $0.5 \mu\text{mol L}^{-1}$ CO_2 in the center

when assuming a $CO_2 : HCO_3^-$ uptake ratio of 10% : 90%. In this case, a larger contribution of CO_2 to total carbon uptake would completely deplete CO_2 in the aggregate center. For comparison, carbonate chemistry gradients were also modeled for a *Trichodesmium* aggregate (ID T1) collected in the North Pacific Subtropical Gyre, where bulk DIC concentrations and total alkalinity are significantly higher. In this aggregate, HCO_3^- and CO_2 gradients were smaller, with a decrease by

60 $\mu\text{mol L}^{-1}$ HCO_3^- and 3 $\mu\text{mol L}^{-1}$ CO_2 toward the aggregate center, reaching 5.5 $\mu\text{mol L}^{-1}$ CO_2 in the center when assuming a $\text{CO}_2 : \text{HCO}_3^-$ uptake ratio of 20% : 80%.

Notably, very large and productive aggregates could not be reproduced by the model, potentially indicating that the high rates of photosynthesis we observed in some aggregates cannot be sustained by inorganic carbon supply (diffusion and reactions) on the long term (i.e., in a steady state). For *Trichodesmium* and *Dolichospermum*, only a PQ below 1 (0.8; Fig. 3) could explain the ratio of measured O_2 and pH gradients, in agreement with previous reports of PQ values for *Trichodesmium* (e.g., PQ 0.45–0.61, Carpenter and Roenneberg 1995; PQ 1.0, Boatman et al. 2019). The slight underestimation of pH deviations by the model even at these low PQ levels (Fig. 3) might indicate the existence of a proton sink associated with photosynthesis that is not accounted for in the model. For *Nodularia*, in contrast, a high PQ was necessary to reproduce the data (1.7; Fig. 3), since otherwise CO_2 concentrations in the aggregate were negative, indicating that cellular carbon uptake (as estimated from measured O_2 gradients using the PQ) could not be supported by diffusion and reactions. It should be noted that these PQ values describe the net O_2 and CO_2 evolution and uptake rates of the whole microbial consortium that forms the aggregate and may therefore be affected by respiration of “old” particulate organic matter or dissolved organic matter (DOM) originating from the surrounding water by heterotrophic bacteria (see the Discussion section).

O_2 and pH microenvironments under elevated $p\text{CO}_2$

In another series of measurements, microenvironment pH and O_2 gradients were determined in cyanobacterial aggregates after experimentally manipulating external $p\text{CO}_2$ levels. In addition to the immediate responses to the change in $p\text{CO}_2$ (instantaneous effects), we investigated the response to incubating the cyanobacteria at the respective $p\text{CO}_2$ for several days (acclimatization effects).

For characterizing instantaneous responses to elevated $p\text{CO}_2$, the seawater in the flow system was bubbled with CO_2 -enriched air, reaching the new $p\text{CO}_2$ level over a time scale of 1–2 h. Conditions in the center of aggregates as well as O_2 evolution and uptake rates under elevated $p\text{CO}_2$ are summarized in Table 3. As a result of the $p\text{CO}_2$ treatment, pH levels in the center of these aggregates were lower than those measured on fresh aggregates under present-day $p\text{CO}_2$ (t -test, $p < 0.05$, $n = 3$ –7). Under elevated $p\text{CO}_2$, pH levels in the center of aggregates ranged between 7.3 (measured in the dark) and 9.2 (measured in the light) with bulk pH levels of 7.7–7.9. Neither the difference in proton concentration in light vs. dark nor volume- or aggregate-specific O_2 concentrations or production and uptake rates were significantly different from those measured on fresh aggregates under present-day $p\text{CO}_2$ (t -test, $p < 0.05$, $n = 3$ –6; Tables 2, 3, S4).

When analyzing the response of individual aggregates to the change in $p\text{CO}_2$, however, it becomes evident that rates of

photosynthesis and respiration generally decreased for both species in response to the instantaneous shift in $p\text{CO}_2$ (10 out of 12 cases; Table 3). This decrease occurred irrespective of the direction of the shift, that is, when freshly collected aggregates were shifted to future $p\text{CO}_2$ (aggregates D1–D6, N1, N4; Table 3; Fig. 4a–c) as well as when aggregates were shifted to present-day $p\text{CO}_2$ after an initial measurement at future $p\text{CO}_2$ (aggregates D7 and N5; Table 3; Fig. 4d–f), suggesting that the decrease was a general stress response rather than a response specific to the future $p\text{CO}_2$ level. Repeated measurements on the same aggregate under constant bulk conditions generally yielded similar results (data not shown), confirming that the observed changes were biological responses to the change in $p\text{CO}_2$ rather than artifacts of repeated measurements on the same aggregate.

For all but one aggregate, the range in proton concentrations in light vs. dark ($d[\text{H}^+]$) was higher under elevated $p\text{CO}_2$ than at present-day conditions (Table 3; Fig. 4c,f). This effect can be attributed to the lower buffer capacity of the carbonate system (Hauck and Völker 2015), which causes a larger change in proton concentration for the same amount of carbon uptake at elevated $p\text{CO}_2$ (see model calculations and the Discussion section below). Notably, we were able to observe this increase in $d[\text{H}^+]$ even when metabolic activity, as revealed by O_2 fluxes, decreased or stayed similar upon the switch to elevated $p\text{CO}_2$ (aggregates D2, D3, N1; Table 3; Fig. 4).

For assessing the effects of acclimatization to the altered $p\text{CO}_2$ condition, aggregates of *Nodularia* and *Dolichospermum* were incubated in roller tanks under different $p\text{CO}_2$ levels for 3–4 d. To test for potential adverse effects of the incubation itself (“bottle effects”), conditions in the center of the aggregate as well as rates of photosynthesis and respiration were compared between freshly collected aggregates and those incubated in a similar manner under present-day in situ $p\text{CO}_2$ conditions. This comparison yielded no significant difference for any of the measured parameters (t -test, $p > 0.05$, $n = 4$). While overall variability between colonies was high, comparing $p\text{CO}_2$ treatments, neither pH levels or the range of proton concentrations in light vs. dark nor volume- or aggregate-specific O_2 concentrations in the center or O_2 uptake and production rates (i.e., respiration and photosynthesis) were significantly different between $p\text{CO}_2$ levels (t -test, $p > 0.05$, $n = 3$ –4; Table 4).

Notably, these measurements on cyanobacterial aggregates reflect the integrated effects of the chemical changes after re-equilibration of the carbonate system with air of higher $p\text{CO}_2$, that is, the shift in the carbonate system toward a higher $\text{CO}_2 : \text{HCO}_3^-$ ratio and the related changes in buffer capacity, as well as the biological responses to these changes. The abiotic effects could be resolved with microsensor measurements on agar spheres containing yeast, representing a nonphotosynthetic biological system that is potentially not as sensitive to $p\text{CO}_2$ levels as the cyanobacterial aggregates (Fig. S2). In this system, while the yeast was actively respiring under both $p\text{CO}_2$ treatments, the gradient in proton concentration was hardly detectable at ambient $p\text{CO}_2$, whereas at future $p\text{CO}_2$, proton

Table 3. Conditions in the center of aggregates of *Dolichospermum* and *Nodularia* as well as O₂ evolution (light) or uptake (dark) rates measured under elevated bulk pCO₂ levels. d[H⁺] indicates the difference in proton concentration in light vs. dark. Columns denoted “Shift resp.” show the ratio between values (of d[H⁺], O₂ evolution or uptake rates, respectively) measured at future pCO₂ to those measured at present-day pCO₂. Aggregates were analyzed first at ambient pCO₂ and then at future pCO₂, except for values labeled with an asterisk, where aggregates were analyzed first at future pCO₂. n.a., not available.

Species	ID	Bulk pH	Light cond.	pH in center	d[H ⁺] in center		[O ₂] in center	O ₂ evolution or uptake rate			
					nmol L ⁻¹	Shift resp.	μmol L ⁻¹	nmol h ⁻¹ aggr. ⁻¹	Shift resp.	nmol h ⁻¹ mm ⁻³	
<i>Dolichospermum</i>	D1	7.9	Light	8.2	9	0.8	345	0.3	0.2	3.0	
			Dark	7.8			305	0.5	0.8	3.9	
	D2	7.8	Light	8.0	13	2.3	357	0.8	0.9	1.8	
			Dark	7.6			308	0.7	1.1	1.3	
	D3	7.9	Light	8.4	23	2.1	382	1.8	0.4	6.5	
			Dark	7.6			291	0.9	0.7	2.1	
	D4	7.8	Light	8.2	n.a.	n.a.	n.a.	n.a.	n.a.	n.a.	
			Dark	n.a.			n.a.	n.a.	n.a.	n.a.	
	D5	7.8	Light	8.2	18	n.a.	n.a.	n.a.	n.a.	n.a.	
			Dark	7.6			n.a.	n.a.	n.a.	n.a.	
	D6	7.7	Light	8.5	15	n.a.	n.a.	n.a.	n.a.	n.a.	
			Dark	7.7			n.a.	n.a.	n.a.	n.a.	
	D7	7.8	Light	9.2	49	1.9*	615	32.0	1.1*	15.6	
			Dark	7.3			167	9.2	1.3*	5.0	
Avg ± SD			Light	8.4±0.4	21±15		425±128	8.8±15.6		6.7±6.3	
			Dark	7.6±0.2			268±68	2.8±4.3		3.1±1.7	
<i>Nodularia</i>	N1	7.8	Light	8.2	25	1.4	375	0.9	1.3	14.5	
			Dark	7.5			280	0.8	0.6	6.2	
	N4	7.9	Light	9.0	n.a.	n.a.	468	6.6	0.6	9.0	
			Dark	n.a.			n.a.	n.a.	n.a.	n.a.	
	N5	7.9	Light	8.5	26	5.0*	417	4.5	2.4*	4.8	
			Dark	7.5			n.a.	n.a.	n.a.	n.a.	
	Avg ± SD			Light	8.6±0.4	26±1		420±47	4.0±2.9		9.5±4.9
				Dark	7.5±0.0			280	0.8		6.2
Total	Avg ± SD		Light	8.4±0.4	22±12		423±94	6.7±11.4		7.9±5.4	
			Dark	7.6±0.2			269±53	2.4±3.8		3.7±2.0	

concentration in the center of the agar spheres was clearly reduced compared to outside (Fig. S2). These results reflect the effects of lower buffer capacity at elevated pCO₂, which leads to a larger change in proton concentration for the same rate of respiration. In the next step, we aimed to dissect these chemical effects from biological responses by model calculations of carbonate chemistry in the aggregate microenvironment.

Microenvironment carbonate chemistry under elevated pCO₂

For a quantitative analysis of the chemical changes in aggregate carbonate chemistry under elevated pCO₂, we modeled the gradients of individual carbon species for two different pCO₂ levels in seawater of different composition (Baltic vs. Pacific), assuming the same rate of photosynthesis in all cases (Fig. 5). In the Baltic seawater scenario with lower

alkalinity and DIC, bulk as well as microenvironment CO₂, HCO₃⁻ and H⁺ concentrations are all lower than in the Pacific scenario. The minimum CO₂ concentration in the center of aggregates was 3.5 μmol L⁻¹ at Baltic present-day conditions as opposed to 9.3 μmol L⁻¹ at Pacific present-day conditions. The deviations in CO₂ and H⁺ in the center of the aggregate as compared to the bulk, in turn, are larger in Baltic than in Pacific seawater despite the same carbon uptake rate assumed in the model. In both Baltic and Pacific seawater, ocean acidification increased not only the CO₂ concentration in the center, but also the deviation in CO₂ and H⁺ concentration from bulk conditions. The magnitude of this effect, however, is larger in the Baltic Sea scenario due to the reduced buffer capacity.

Previous model results have demonstrated that eCA activity can substantially modify carbonate chemistry gradients in the

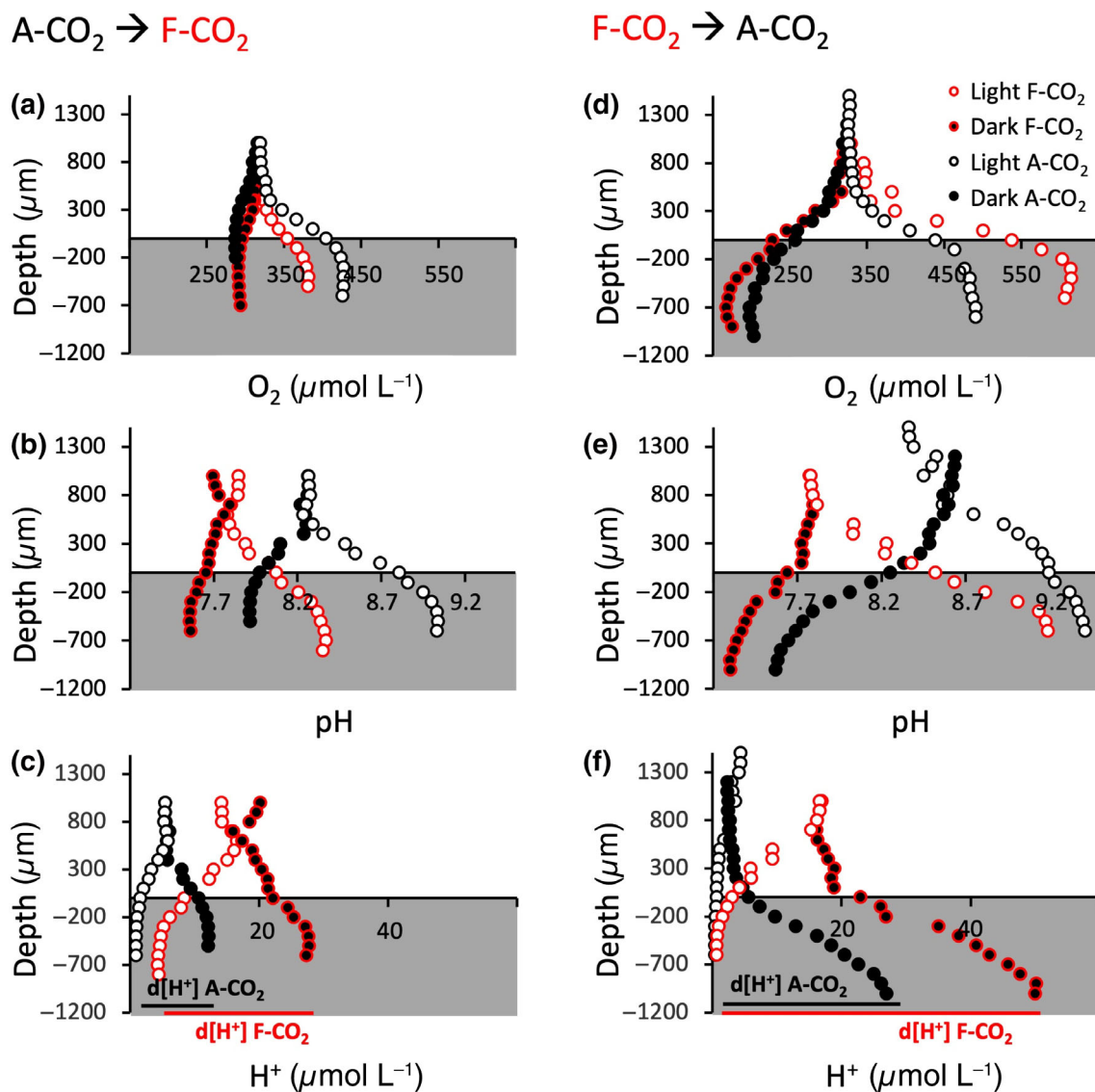


Fig 4. Examples of depth profiles showing effects of short-term $p\text{CO}_2$ shifts on gradients of O_2 , pH, and H^+ concentration within and around aggregates of *Dolichospermum*. Approximate area taken by the aggregate is indicated by gray shading. (a–c) Aggregate shifted from present-day to future $p\text{CO}_2$ (aggregate D3). (d–f) Aggregate shifted from future to present-day $p\text{CO}_2$ (aggregate D7). A- CO_2 , ambient $p\text{CO}_2$; F- CO_2 , future $p\text{CO}_2$.

Table 4. Conditions in the center of aggregates of *Dolichospermum* and *Nodularia* as well as O_2 evolution (light) or uptake (dark) rates measured after acclimatization to different $p\text{CO}_2$ conditions for 3–4 d. $d[\text{H}^+]$ indicates the difference in proton concentration in light vs. dark. $n = 4$, except for O_2 uptake at F- CO_2 in the dark with $n = 3$. A- CO_2 , ambient $p\text{CO}_2$; F- CO_2 , future $p\text{CO}_2$.

Bulk pH	Light cond.	pH in center	$d[\text{H}^+]$ in center	$[\text{O}_2]$ in center	O_2 evolution or uptake rate	
					nmol L^{-1}	$\mu\text{mol L}^{-1}$
A- CO_2	Light	8.9 ± 0.2	31 ± 24	446 ± 69	7 ± 4	7 ± 5
	Dark	7.6 ± 0.3		227 ± 59	5 ± 3	3 ± 2
F- CO_2	Light	8.5 ± 0.5	33 ± 21	418 ± 75	5 ± 2	9 ± 8
	Dark	7.4 ± 0.2		263 ± 55	4 ± 2	3 ± 1

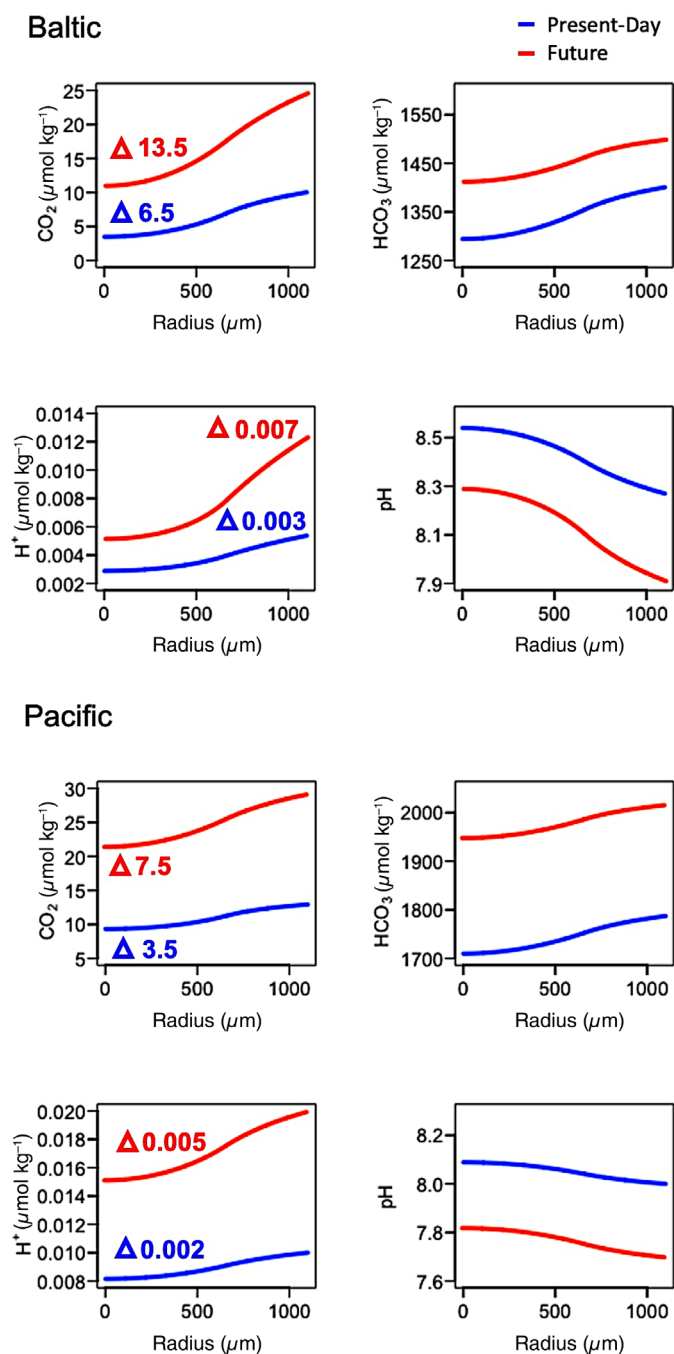


Fig 5. Modeled carbonate chemistry gradients in the microenvironment of an aggregate with the same biological activity under different bulk conditions representing present-day and future scenarios for Baltic vs. Pacific seawater. Size and total carbon uptake as measured on *Dolichospermum* aggregate D2 (Fig. 3). Other input parameter values as specified in Table S2. Numbers in the plots indicate the deviation in the center of the aggregate from bulk conditions in $\mu\text{mol kg}^{-1}$.

diffusive boundary layer around diatom cells (Chrachri et al. 2018). While to the best of our knowledge, there is no evidence for eCA in *N. spumigena* or *Dolichospermum*, eCA activity or genetic potential have been occasionally reported

in other cyanobacteria (Soltes-Rak et al. 1997; Li et al. 2018). To investigate the potential effects of eCA activity on carbonate chemistry within aggregates, we implemented the effects of an acceleration of the conversion between CO_2 and HCO_3^- in our model (Fig. S3). Under Pacific seawater conditions, eCA effects were negligible, while under present-day Baltic conditions, for an acceleration of the conversion by a factor of 10^7 (Radzicka and Wolfenden 1995) our model predicts ca. 30% lower CO_2 concentrations in the aggregate center. Under future Baltic conditions, eCA effects were stronger, reaching negative CO_2 concentrations in the aggregate center at acceleration factors of 10^5 . Hence, if eCA was active in *Nodularia* and *Dolichospermum*, stronger drawdown of CO_2 but slightly less pronounced pH increase in the aggregate could be expected compared to the situation without eCA activity (Figs. S3, 5).

Discussion

The period of this field study encompassed the typical chemical, physical, and biological changes occurring over the development of cyanobacterial blooms in the Baltic Sea, giving us the opportunity to sample aggregates of two of the major N_2 -fixing cyanobacteria in this system under a wide range of in situ carbonate chemistry conditions. $p\text{CO}_2$ decreased from 350 to 130 μatm and pH rose from 8.2 to 8.6 due to photosynthesis as the biomass of *Nodularia* and *Dolichospermum* increased (Table 1). In the following, we summarize our findings on O_2 , pH, and carbonate chemistry within these cyanobacterial aggregates, discuss the main processes that shape these microenvironments, and evaluate their physiological implications under present-day and future conditions.

Players and processes behind O_2 and pH gradients

Over the course of our study, the dominant species of cyanobacteria at the surface shifted between *Nodularia* and *Dolichospermum* (Table 1). In this—to our knowledge—first report of microsensor measurements on *Dolichospermum* aggregates, O_2 and pH microenvironments as well as net O_2 fluxes in light and dark were similar between these two species (Table 2). In addition to these large cyanobacteria, a variable number of other phytoplankton cells including diatoms, dinoflagellates, other cyanobacteria and protozoans were observed in the aggregates (not shown), and an average of 35 presumably heterotrophic epibionts per cell of *Nodularia* were found in a study conducted at the same time and location (Schoffelen et al. 2019). Notably, the O_2 and CO_2 fluxes shown here reflect the combined activity of this microbial consortium.

Turnover of carbon within the aggregate through close coupling of DOM production by the cyanobacteria and subsequent CO_2 release by respiring associated bacteria can be substantial. For instance, previous microsensor measurements

on strongly net autotrophic Baltic aggregates showed that O_2 uptake in the light can exceed the O_2 flux into the aggregate in the dark by a factor of > 5 due to recycling of O_2 and CO_2 in the aggregate interior, which can be driven by photorespiration (RubisCO functioning as an oxygenase) and/or intense recycling of carbon and O_2 between the autotrophic and heterotrophic microorganisms within the aggregate (Ploug 2008). Importantly, this recycling of O_2 and CO_2 does not lead to net fluxes of O_2 and CO_2 between the cyanobacterial aggregate and the ambient water when the DOM is freshly produced and released by the cyanobacteria (Fig. 1). In contrast, DOM derived from “old” particulate organic matter or diffusion of DOM from the surrounding water into the aggregate would lead to net O_2 consumption and CO_2 production in the interior of aggregates. These latter processes would thus affect steady state gradients of O_2 and carbon in and around the aggregates but are not explicitly included in our diffusion-reaction model.

In summary, the O_2 fluxes calculated from *steady state* O_2 concentration gradients at the aggregate surface in light and dark shown in this study (Tables 2–4) reflect the net fluxes of O_2 in and out of the aggregate that result from the interplay of various processes (Fig. 1). In agreement with previous studies on cyanobacterial aggregates (Ploug et al. 2011; Eichner et al. 2020), these net O_2 fluxes differed strongly between individual aggregates, resulting in large variability even when considering volume-normalized rates (Tables 2–4).

Generally, these data revealed that the microbial consortium as a whole in both aggregate types was strongly net autotrophic in light, which was also reflected in the pH gradients. Dark O_2 respiration rates were equivalent to approximately a third of gross photosynthesis, which is relatively high compared to other phytoplankton, but similarly high ratios have been reported previously on *Nodularia* aggregates (0.20–0.38; Ploug et al. 2011). The high dark respiration relative to gross photosynthesis may reflect respiration of “old” particulate organic matter or DOM originating from the surrounding water by associated bacteria and other organisms in the aggregate consortium and/or the energy costs related to N_2 fixation and use of dissolved organic phosphorus by the N_2 -fixing cyanobacteria (Schoffelen et al. 2018).

Inorganic carbon gradients in different seawater systems

Carbon uptake and respiration induced distinct micrometer-scale pH gradients within the aggregate microenvironment, in agreement with previous studies on Baltic and Pacific cyanobacteria (Ploug 2008; Eichner et al. 2017). Here, we show by model calculations that such changes in pH reflect decreases in the order of 100–150 $\mu\text{mol L}^{-1} \text{HCO}_3^-$ and 3–6 $\mu\text{mol L}^{-1} \text{CO}_2$ in the aggregate center due to carbon uptake in the light (Figs. 3, 5). Especially in the Baltic Sea

under bloom conditions when bulk CO_2 levels decrease, this can lead to almost complete drawdown of CO_2 concentrations in the aggregate center (Fig. 3; $< 1 \mu\text{mol L}^{-1} \text{CO}_2$).

Variations in photosynthetic activity, which could be induced by changing light intensity either on short time scales with mixing and/or sudden changes in cloud cover or over the day–night cycle can thus induce highly variable microenvironment carbonate chemistry over time. For a given biological activity, the lower alkalinity of Baltic seawater causes such variations to be more pronounced in Baltic aggregates than in Pacific *Trichodesmium* aggregates (Fig. 5). Yet, despite the different seawater composition and the large size difference between *Trichodesmium* and Baltic aggregates, pH and O_2 saturation measured in the microenvironment were not significantly different between these types of aggregates, probably as a result of species-specific differences in biological activity but also large variation between activities of individual aggregates (Tables 2, S4).

pH gradients under future $p\text{CO}_2$: Abiotic vs. biotic effects

Our model calculations and measurements on yeast showed stronger gradients in proton concentrations within aggregates under future $p\text{CO}_2$, which reflects the lower buffer capacity under ocean acidification (Fig. 5). In a previous model study, this effect was proposed to induce larger pH variability in the microenvironments of single cells in the future, yet that study did not account for physiological responses to $p\text{CO}_2$ that may alter cellular carbon uptake rates (Flynn et al. 2012). Here, we combined model calculations and microsensor measurements on cyanobacterial aggregates, which allowed us to dissect the chemical and biological effects of the change in $p\text{CO}_2$. Based on pH and O_2 microsensor measurements on individual aggregates at different $p\text{CO}_2$ levels, we show that the larger variability in proton gradients at future $p\text{CO}_2$ was manifested even when the cyanobacteria reduced their photosynthetic activity in response to the instantaneous change in $p\text{CO}_2$ (Fig. 4).

The reduction in activity as an immediate stress response to our $p\text{CO}_2$ treatment shows that both *Nodularia* and *Dolichospermum* are sensitive to short-term changes in carbonate chemistry (time-scale of hours). In their natural environment, mixing, aggregation, and formation of surface scums or the feedbacks of photosynthesis rates changing with light intensity may induce changes in microenvironment carbonate chemistry on similarly short time scales. Under such conditions, an ability to quickly recover from environmental changes is important. In line with this, over acclimatization time scale (several days), there was no significant difference between $p\text{CO}_2$ treatments, yet it should be noted that such an effect may have been masked by the large variability between individual aggregates.

Potential for downregulation of the CCM

By means of their CCM, cyanobacteria can concentrate CO₂ within the carboxysome in order to saturate RubisCO (Badger and Price 2003). Previous studies have demonstrated that activity of the CCM is adjusted in response to changes in external carbonate chemistry (Eichner et al. 2015). As the cells strive to achieve a given degree of RubisCO saturation at the minimal possible cost at all times, changes in external CO₂ concentration can thus result in energy savings for the CCM. At a constant ratio of CO₂ to HCO₃⁻ uptake of 20% CO₂ contribution to total C_i uptake, under ocean acidification the CO₂ concentration in the center of the aggregate would increase from 3.5 to 11.0 μmol L⁻¹ in the Baltic Sea scenario, and from 9.3 to 21.4 μmol L⁻¹ in the Pacific seawater scenario (Table 5). Assuming that the CCM is adjusted to saturate RubisCO by more than 80% to reach an intracellular CO₂ concentration of ca. 1000 μmol L⁻¹ in all cases (following estimates for *Trichodesmium*; Eichner et al. 2015), these changes in external CO₂ concentration would decrease the required accumulation factor (CO₂ at RubisCO : external CO₂) from 286 to 91 in the Baltic scenario, and from 108 to 47 in the Pacific scenario (Table 5).

While CO₂ can freely diffuse into the cell, HCO₃⁻ can only be taken up by ATP- or Na⁺-dependent transporters (Badger and Price 2003). Assuming a scenario without eCA, where the cells increase the ratio of CO₂ to HCO₃⁻ uptake up to the point where CO₂ is fully depleted in the center of the aggregate, we calculated the maximum possible contribution of CO₂ to total inorganic carbon uptake for each scenario (Table 5). In the Pacific scenario, carbon uptake could be fully supported by CO₂ under both present-day and ocean acidification conditions, with 6.3 μmol L⁻¹ CO₂ remaining in the center at present-day conditions. In the Baltic scenario, the maximum contribution of CO₂ to total uptake could be increased from 45% under present-day to 95% under ocean acidification conditions. This equals decreasing the rate of HCO₃⁻ uptake by a factor of 10, which would significantly decrease the energy costs for the CCM.

Notably, the concentrations to which the CCM can draw down CO₂ ultimately depends on the CO₂ affinity of the NDH-1 complex that converts CO₂ to HCO₃⁻ in the cytoplasm (Price et al. 2008) and the concentration gradient across the cell wall that is necessary to maintain diffusive influx into the cytoplasm. Previous measurements of cellular inorganic carbon fluxes in *Trichodesmium* suggested net CO₂ efflux (Eichner et al. 2015), that is, elevated CO₂ concentrations in the cytoplasm compared to outside, which could prevent efficient diffusive CO₂ uptake even at CO₂ concentrations far above zero. This could potentially explain why previous observations by membrane inlet mass spectrometry showed much lower CO₂ contributions to carbon uptake (< 20%; Eichner et al. 2015) than the maximum possible contribution estimated here (Table 5).

Implications for ocean acidification responses

The strong CO₂ drawdown in aggregate microenvironments suggests that aggregates may benefit more than single filaments or cells from elevated pCO₂ under ocean acidification. A flexible CCM with a variable proportion of HCO₃⁻ uptake, as required for economic energy management under the low and highly variable CO₂ concentrations in Baltic aggregates (Figs. 3–5; Table 5), may make Baltic cyanobacteria particularly efficient in harvesting energy savings under ocean acidification. However, the associated changes in pH have various additional effects on the physiology of N₂ fixers.

Recent studies on ocean acidification responses of *Trichodesmium* highlighted the fine balance between the benefit of elevated pCO₂ for carbon uptake on the one hand, and the inhibition of nitrogenase by low pH, which induced increased energy investment into nitrogenase synthesis, on the other hand (Shi et al. 2012; Luo et al. 2019).

In aggregates, such inhibitory effects might be expected especially at night when pH levels are lower than in the bulk due to respiration (Figs. 2, 4; Table 3). While nitrogenase activity is low at this time, as indicated by low nighttime N₂

Table 5. Overview of CCM requirements for three representative aggregates (cf. Fig. 3) under different carbonate chemistry scenarios (cf. Fig. 5). The accumulation factor was calculated assuming a CO₂ concentration in the vicinity of RubisCO of 1000 μmol L⁻¹, following previous estimations based on the K_M of RubisCO (Badger et al. 1998) and cellular carbon affinity (Eichner et al. 2015). The maximum possible CO₂ contribution is calculated as the ratio of CO₂ uptake to total inorganic carbon uptake yielding a CO₂ concentration < 0.5 μmol L⁻¹ in the center (calculation in steps of 0.05). PQ 0.8 for *Dolichospermum* and *Trichodesmium*, 1.7 for *Nodularia*. DIC, dissolved inorganic carbon.

		Dolichospermum D2				Nodularia N2	Trichodesmium T1
		Baltic		Pacific		Baltic	Pacific
		Present	Future	Present	Future	Present	Present
[CO ₂] in center at 20% CO ₂ uptake	μmol L ⁻¹	3.5	11.0	9.3	21.4	<0	5.7
Accumulation factor		286	91	108	47	—	175
Max. possible CO ₂ contrib.	CO ₂ :DIC	0.45	0.95	1	1	0.1	0.75
[CO ₂] in center at max. CO ₂ contrib.	μmol L ⁻¹	<0.5	<0.5	6.2	18.8	<0.5	<0.5

fixation rates observed in both *Nodularia* (Ploug et al. 2011) and *Trichodesmium* (Eichner et al. 2014a), the synthesis of nitrogenase may be sensitive to nighttime pH as this is when the bulk of daily nitrogenase de novo synthesis occurs in *Trichodesmium* (Capone et al. 1990). In contrast, during daytime, when nitrogenase is active in both *Nodularia* and *Trichodesmium*, pH levels in the center of the aggregate under ocean acidification are similar to those in the bulk under present-day conditions (Fig. 5), suggesting that aggregates may provide a “pH refugium” for nitrogenase under ocean acidification. In line with this, in the field-collected *Trichodesmium* colonies modeled in this study, N₂ fixation was elevated upon treatment with high pCO₂ levels during daytime (Eichner et al. 2017).

Overall, aggregate formation thus leads to milder acidification during daytime but more severe acidification at nighttime and the net effect over the diel cycle depends on the fine balance of the various positive and negative effects of these trends. With the lower buffer capacity of Baltic compared to Pacific seawater (Figs. 3, 5), “critical boundaries” in pH with respect to cell physiology might be reached earlier in Baltic aggregates than in *Trichodesmium* colonies. In line with this, a previous literature review suggested that Baltic cyanobacteria were more prone than *Trichodesmium* to show negative responses in growth, particulate organic carbon, and nitrogen production rates as well as N₂ fixation to ocean acidification (Eichner et al. 2014b). In this study, the lack of pCO₂ responses in photosynthesis on acclimatization time scale suggests that the various physiological effects associated with elevated pCO₂ might compensate each other, similar to findings in previous field studies on *Trichodesmium* (Böttjer et al. 2014; Eichner et al. 2017).

Conclusions

Combining microsensor measurements and model calculations, we were able to quantitatively describe the gradients in O₂, pH, and the individual carbon species within cyanobacterial aggregates. The magnitude of the deviations in CO₂ and pH from bulk conditions induced by photosynthesis and respiration depends on the composition of the seawater; hence, aggregate-forming cyanobacteria in the Baltic Sea (*Nodularia* and *Dolichospermum*) are subject to stronger deviations in the microenvironment than *Trichodesmium* in the Pacific. In large and productive aggregates of *Nodularia* and *Dolichospermum*, CO₂ can be depleted to below 1 μmol L⁻¹ even when ≥ 80% of inorganic carbon supply is covered by HCO₃⁻, requiring a large energy investment in the CCM.

Under ocean acidification, the decrease in buffer capacity amplifies gradients in CO₂ and pH especially in Baltic seawater, which was manifested in CO₂ manipulation experiments even when photosynthetic activity decreased in response to elevated pCO₂ levels. Relief of CO₂ limitation within aggregates under ocean acidification can lead to

significant energy savings for the CCM, while overall pH effects depend on the balance between the benefits of high daytime pH levels, possibly providing a refuge from ocean acidification in the aggregate, and potential adverse effects of low nighttime pH levels.

References

- Badger, M. R., T. J. Andrews, S. M. Whitney, M. Ludwig, and D. C. Yellowlees. 1998. The diversity and co-evolution of Rubisco, plastids, pyrenoids and chloroplast-based CO₂-concentrating mechanisms in algae. *Can. J. Bot.* **76**: 1052–1071.
- Badger, M. R., and G. D. Price. 2003. CO₂ concentrating mechanisms in cyanobacteria: Molecular components, their diversity and evolution. *J. Exp. Bot.* **54**: 609–622.
- Badger, M. R., G. D. Price, B. M. Long, and F. J. Woodger. 2006. The environmental plasticity and ecological genomics of the cyanobacterial CO₂ concentrating mechanism. *J. Exp. Bot.* **57**: 249–265.
- Boatman, T. G., P. A. Davey, T. Lawson, and R. J. Geider. 2019. CO₂ modulation of the rates of photosynthesis and light-dependent O₂ consumption in *Trichodesmium*. *J. Exp. Bot.* **70**: 589–597.
- Böttjer, D., D. M. Karl, R. M. Letelier, D. A. Viviani, and M. J. Church. 2014. Experimental assessment of diazotroph responses to elevated seawater pCO₂ in the North Pacific subtropical gyre. *Global Biogeochem. Cycles* **28**: 601–616.
- Broecker, W. S., and T.-H. Peng. 1974. Gas exchange rates between air and sea. *Tellus* **26**: 21–35.
- Burnap, R. L., M. Hagemann, and A. Kaplan. 2015. Regulation of CO₂ concentrating mechanism in cyanobacteria. *Life* **5**: 348–371.
- Capone, D. G., J. M. O’Neil, J. Zehr, and E. J. Carpenter. 1990. Basis for diel variation in nitrogenase activity in the marine planktonic cyanobacterium *Trichodesmium thiebautii*. *Appl. Environ. Microbiol.* **56**: 3532–3536.
- Carpenter, E. J., and T. Roenneberg. 1995. The marine planktonic cyanobacteria *Trichodesmium* spp - photosynthetic rate measurements in the SW Atlantic Ocean. *Mar. Ecol.-Prog. Ser.* **118**: 267–273.
- Chrachri, A., B. M. Hopkinson, K. Flynn, C. Brownlee, and G. L. Wheeler. 2018. Dynamic changes in carbonate chemistry in the microenvironment around single marine phytoplankton cells. *Nat. Commun.* **9**: 74.
- Dickson, A. G., C. L. Sabine, and J. R. Christian. 2007. Guide to best practices for ocean CO₂ measurements. North Pacific Marine Science Organization.
- Doney, S. C., V. J. Fabry, R. A. Feely, and J. A. Kleypas. 2009. Ocean acidification: The other CO₂ problem. *Ann. Rev. Mar. Sci.* **1**: 169–192.
- Egleston, E. S., C. L. Sabine, and F. M. Morel. 2010. Revelle revisited: Buffer factors that quantify the response of ocean

- chemistry to changes in DIC and alkalinity. *Global Biogeochem. Cycles* **24**: 1–9.
- Eichner, M., S. Basu, S. Wang, D. de Beer, and Y. Shaked. 2020. Mineral iron dissolution in *Trichodesmium* colonies: The role of O₂ and pH microenvironments. *Limnol. Oceanogr.* **65**: 1149–1160.
- Eichner, M., S. A. Kranz, and B. Rost. 2014a. Combined effects of different CO₂ levels and N sources on the diazotrophic cyanobacterium *Trichodesmium*. *Phys. Plant.* **152**: 316–330.
- Eichner, M., B. Rost, and S. A. Kranz. 2014b. Diversity of ocean acidification effects on marine N₂ fixers. *J. Exp. Mar. Biol. Ecol.* **457**: 199–207.
- Eichner, M., S. Thoms, S. A. Kranz, and B. Rost. 2015. Cellular inorganic carbon fluxes in *Trichodesmium*: A combined approach using measurements and modelling. *J. Exp. Bot.* **66**: 749–759.
- Eichner, M. J., and others. 2017. Chemical microenvironments and single-cell carbon and nitrogen uptake in field-collected colonies of *Trichodesmium* under different pCO₂. *ISME J.* **11**: 1305–1317.
- Flynn, K. J., and others. 2012. Changes in pH at the exterior surface of plankton with ocean acidification. *Nat. Clim. Change* **2**: 510–513.
- Hauck, J., and C. Völker. 2015. Rising atmospheric CO₂ leads to large impact of biology on Southern Ocean CO₂ uptake via changes of the Revelle factor. *Geophys. Res. Lett.* **42**: 1459–1464.
- Kaplan, A. 2017. On the cradle of CCM research: Discovery, development, and challenges ahead. *J. Exp. Bot.* **68**: 3785–3796.
- Klawonn, I., S. Bonaglia, V. Brüchert, and H. Ploug. 2015. Aerobic and anaerobic nitrogen transformation processes in N₂-fixing cyanobacterial aggregates. *ISME J.* **9**: 1456–1466.
- Kranz, S. A., D. Sültemeyer, K.-U. Richter, and B. Rost. 2009. Carbon acquisition in *Trichodesmium*: The effect of pCO₂ and diurnal changes. *Limnol. Oceanogr.* **54**: 548–559.
- Kranz, S. A., D. Wolf-Gladrow, G. Nehrke, G. Langer, and B. Rost. 2010. Calcium carbonate precipitation induced by the growth of the marine cyanobacteria *Trichodesmium*. *Limnol. Oceanogr.* **55**: 2563–2569.
- Li, T., C. E. Sharp, M. Ataeian, M. Strous, and D. De Beer. 2018. Role of extracellular carbonic anhydrase in dissolved inorganic carbon uptake in alkaliphilic phototrophic biofilm. *Front. Microbiol.* **9**: 2490.
- Long, B. M., B. D. Rae, V. Rolland, B. Förster, and G. D. Price. 2016. Cyanobacterial CO₂-concentrating mechanism components: Function and prospects for plant metabolic engineering. *Curr. Opin. Plant Biol.* **31**: 1–8.
- Luo, Y.-W., D. Shi, S. A. Kranz, B. M. Hopkinson, H. Hong, R. Shen, and F. Zhang. 2019. Reduced nitrogenase efficiency dominates response of the globally important nitrogen fixer *Trichodesmium* to ocean acidification. *Nat. Commun.* **10**: 1–12.
- Millero, F. J., R. Woosley, B. DiTrollo, and J. Waters. 2009. Effect of ocean acidification on the speciation of metals in seawater. *Oceanography* **22**: 72–85.
- Morel, F. M., and J. G. Hering. 1993. Principles and applications of aquatic chemistry. John Wiley & Sons.
- Müller, J. D., B. Schneider, and G. Rehder. 2016. Long-term alkalinity trends in the Baltic Sea and their implications for CO₂-induced acidification. *Limnol. Oceanogr.* **61**: 1984–2002.
- Omstedt, A., C. Humborg, J. Pempkowiak, M. Perttilä, A. Rutgersson, B. Schneider, and B. Smith. 2014. Biogeochemical control of the coupled CO₂–O₂ system of the Baltic Sea: A review of the results of Baltic-C. *Ambio* **43**: 49–59.
- Pierrot, D., E. Lewis, and D. Wallace. 2006. MS Excel program developed for CO₂ system calculations. ORNL/CDIAC-105. Carbon Dioxide Information Analysis Center, Oak Ridge National Laboratory, US Department of Energy.
- Ploug, H. 2008. Cyanobacterial surface blooms formed by *Aphanizomenon* sp. and *Nodularia spumigena* in the Baltic Sea: Small-scale fluxes, pH, and oxygen microenvironments. *Limnol. Oceanogr.* **53**: 914–921.
- Ploug, H., B. Adam, N. Musat, T. Kalvelage, G. Lavik, D. Wolf-Gladrow, and M. M. Kuypers. 2011. Carbon, nitrogen and O₂ fluxes associated with the cyanobacterium *Nodularia spumigena* in the Baltic Sea. *ISME J.* **5**: 1549–1558.
- Ploug, H., and B. B. Jørgensen. 1999. A net-jet flow system for mass transfer and microsensor studies of sinking aggregates. *Mar. Ecol. Prog. Ser.* **176**: 279–290.
- Ploug, H., M. Kühl, B. Buchholz-Cleven, and B. B. Jørgensen. 1997. Anoxic aggregates—an ephemeral phenomenon in the pelagic environment? *Aquat. Microb. Ecol.* **13**: 285–294.
- Price, G. D., M. R. Badger, F. J. Woodger, and B. M. Long. 2008. Advances in understanding the cyanobacterial CO₂-concentrating-mechanism (CCM): Functional components, C_i transporters, diversity, genetic regulation and prospects for engineering into plants. *J. Exp. Bot.* **59**: 1441–1461.
- Radzicka, A., and R. Wolfenden. 1995. A proficient enzyme. *Science* **267**: 90–93.
- Rost, B., S. A. Kranz, K. U. Richter, and P. D. Tortell. 2007. Isotope disequilibrium and mass spectrometric studies of inorganic carbon acquisition by phytoplankton. *Limnol. Oceanogr.: Methods* **5**: 328–337.
- Schneider, B., K. Eilola, K. Lukkari, B. Muller-Karulis, and T. Neumann. 2015. Environmental impacts—marine biogeochemistry, p. 337–361. *In* Second assessment of climate change for the Baltic Sea basin. Springer.
- Schoffelen, N. J., W. Mohr, T. G. Ferdelman, J. Duerschlag, S. Littmann, H. Ploug, and M. M. Kuypers. 2019. Phosphate availability affects fixed nitrogen transfer from diazotrophs to their epibionts. *ISME J.* **13**: 2701–2713.
- Schoffelen, N. J., W. Mohr, T. G. Ferdelman, S. Littmann, J. Duerschlag, M. V. Zubkov, H. Ploug, and M. M. Kuypers. 2018. Single-cell imaging of phosphorus uptake shows that

- key harmful algae rely on different phosphorus sources for growth. *Sci. Rep.* **8**: 1–13.
- Shi, D. L., S. A. Kranz, J. M. Kim, and F. M. M. Morel. 2012. Ocean acidification slows nitrogen fixation and growth in the dominant diazotroph *Trichodesmium* under low-iron conditions. *Proc. Natl. Acad. Sci. USA* **109**: E3094–E3100.
- Soltes-Rak, E., M. E. Mulligan, and J. R. Coleman. 1997. Identification and characterization of a gene encoding a vertebrate-type carbonic anhydrase in cyanobacteria. *J. Bacteriol.* **179**: 769–774.
- Wesslander, K., A. Omstedt, and B. Schneider. 2010. Inter-annual and seasonal variations in the air–sea CO₂ balance in the central Baltic Sea and the Kattegat. *Cont. Shelf Res.* **30**: 1511–1521.
- Wolf-Gladrow, D., and U. Riebesell. 1997. Diffusion and reactions in the vicinity of plankton: A refined model for inorganic carbon transport. *Mar. Chem.* **59**: 17–34.
- Wolf-Gladrow, D. A., J. Bijma, and R. E. Zeebe. 1999. Model simulation of the carbonate chemistry in the microenvironment of symbiont bearing foraminifera. *Mar. Chem.* **64**: 181–198.
- Zeebe, R. E., and D. Wolf-Gladrow. 2001. CO₂ in seawater: Equilibrium, kinetics, isotopes. Gulf Professional Publishing.

Acknowledgments

We thank Eva Lindell and the entire staff at Askö Laboratory for their excellent support with sampling and experimental work at Askö, and Volker Brüchert (University of Stockholm) for help with $p\text{CO}_2$ measurements. We also thank Björn Rost and Mandy Kiel (Alfred Wegener Institute Helmholtz Centre for Polar and Marine Research) for DIC and TA measurements. The work was funded by the Alexander von Humboldt Foundation as well as the Royal Society of Arts and Sciences in Gothenburg (KVS), the Swedish Research Council for Environment, Agricultural Sciences and Spatial Planning (FORMAS, grant no. 215-2010-779 to H.P.), and the University of Gothenburg. We thank the two anonymous reviewers for their constructive comments that helped improve the manuscript.

Conflict of Interest

None declared.

Submitted 23 April 2021

Revised 02 November 2021

Accepted 05 November 2021

Associate editor: Ilana Berman-Frank